A Reliable Synthesis of Cubic Mesoporous MCM-48 Molecular Sieve

Jie Xu,[†] Zhaohua Luan,[†] Heyong He,[‡] Wuzong Zhou,[§] and Larry Kevan*,[†]

Department of Chemistry, University of Houston, Houston, Texas 77204-5641, Leverhulme Centre for Innovative Catalysis, Department of Chemistry, University of Liverpool, Liverpool L69 3BX, U. K., and Department of Chemistry, University of Cambridge, Lensfield Road, Cambridge CB2 1EW, U.K.

Received June 22, 1998. Revised Manuscript Received September 17, 1998

Powder X-ray diffraction (XRD), ^{29}Si magic-angle-spinning (MAS) NMR spectroscopy, and transmission electron microscopy (TEM) as well as N_2 adsorption have been employed to study the formation of various mesophases that lead to the synthesis of cubic mesoporous MCM-48 molecular sieve. A typical synthesis is performed at 373 K, pH = 11.8 using tetraethyl orthosilicate as the silicon source and cetyltrimethylammonium bromide (CTAB) as the structure-directing agent with a molar gel composition of 1:0.23:0.55:112SiO_2/Na_2O/CTAB/H_2O. XRD shows that a disordered tubular mesophase (H_1) rapidly forms and then transforms to a layered phase (L_1) upon heating at 373 K for 5−10 h. After the hydrothermal treatment continues for 72 h, the layered phase (L_1) gradually transforms to a cubic MCM-48 mesophase (V), which is accompanied by a slight pH increase of about 0.2 units. Prolonged hydrothermal treatment for over 120 h results in further structural transformation from the cubic mesophase V to a second layered phase (L_2). ^{29}Si MAS NMR reveals that the L_2 layered phase has a more regular atomic arrangement than the other three mesophases. However, the silica condensation increases monotonicly in the order $H_1 \rightarrow L_1 \rightarrow V \rightarrow L_2$ with hydrothermal treatment time. The cubic MCM-48 mesophase is not completely stable under hydrothermal synthesis conditions since it converts to the L_2 phase. This may account for the poor repeatability of prior syntheses of MCM-48 material. We show that cubic MCM-48 can be stabilized either by addition of acetic acid to maintain a constant gel pH or by selection of the reaction time to prevent further mesophase transformation. TEM and N_2 adsorption data show well-defined three-dimensional channels for the cubic MCM-48.

Introduction

A new class of mesoporous molecular sieves called M41S materials with uniform but controllable pore sizes in the range of 20−100 Å initially synthesized using surfactant structure-directing agents[1,2] has attracted much attention.[3,4] The main materials in the M41S family are hexagonal (MCM-41), cubic (MCM-48), and unstable lamellar phases. Other phases such as SBA-n and MSU-n have also been reported.[5−9] MCM-41 and MCM-48 are the most promising for potential applications in catalysis due to their high thermal stability and high adsorption capacity. Most research has concentrated on MCM-41 materials.[3,4,10−16] Fewer publications deal with the synthesis of MCM-48.[17−25] This seems due

[†] University of Houston.
[‡] University of Liverpool.
[§] University of Cambridge.

(1) Kresge, C. T.; Leonowicz, M. E.; Roth, W. J.; Vartuli, J. C.; Beck, J. S. *Nature* **1992**, *359*, 710.
(2) Beck, J. S.; Vartuli, J. C.; Roth, W. J.; Leonowicz, M. E.; Kresge, C. T.; Schmitt, K. D.; Chu, C. T.-W.; Olson, D. H.; Sheppard, E. W.; McCullen, S. B.; Higgins, J. B.; Schlenker, J. L. *J. Am. Chem. Soc.* **1992**, *114*, 10834.
(3) Casci, J. L. In *Advanced Zeolite Science and Application*; Jansen, J. C., Stöcker, M., Karge, H. G., Weitkamp, J., Eds.; Elsevier: Amsterdam, 1994; 329 [*Stud. Surf. Sci. Catal.* **1994**, *85*, 329].
(4) Sayari, A. *Chem. Mater.* **1996**, *8*, 1840.
(5) Huo, Q.; Margolese, D. I.; Ciesla, U.; Feng, P.; Gier, T. E.; Sieger, P.; Leon, R.; Petroff, P. M.; Schüth, F.; Stucky, G. D. *Nature* **1994**, *368*, 317.
(6) Huo, Q.; Leon, R.; Petroff, P. M.; Stucky, G. D. *Science* **1995**, *268*, 1324.
(7) Zhao, D.; Feng, J.; Huo, Q.; Melosh, N.; Fredrickson, G. H.; Chemlka, B. F.; Stucky, G. D. *Science* **1998**, *279*, 548.
(8) Bagshaw, S. A.; Prouzet, E.; Pinnavaia, T. J. *Science* **1995**, *269*, 1242.
(9) Tanev, P. T.; Liang, Y.; Pinnavaia, T. J. *J. Am. Chem. Soc.* **1997**, *119*, 8616.
(10) Vartuli, J. C.; Kresge, C. T.; Leonowicz, M. E.; Chu, A. S.; McCullen, S. B.; Johnson, I. D.; Sheppard, E. W. *Chem. Mater.* **1994**, *6*, 2070.
(11) Beck, J. S.; Vartuli, J. C.; Kennedy, G. J.; Kresge, C. T.; Roth, W. J.; Schramm, S. E. *Chem. Mater.* **1994**, *6*, 1816.
(12) Sayari, A.; Liu, P.; Kruk, M.; Jaroniec, M. *Chem. Mater.* **1997**, *9*, 2499.
(13) Zhao, D.; Luan, Z.; Kevan, L. *J. Chem. Soc., Chem. Commun.* **1997**, 1009.
(14) Luan, Z.; Xu, J.; He, H.; Klinowski, J.; Kevan, L. *J. Phys. Chem.* **1996**, *100*, 19595.
(15) Pöppl, A.; Baglioni, P.; Kevan, L. *J. Phys. Chem.* **1995**, *99*, 14156.
(16) Chen, C. Y.; Burkett, S.; Li, H. X.; Davis, M. E. *Microporous Mater.* **1993**, *2*, 27.
(17) Vartuli, J. C.; Schmitt, K. D.; Kresge, C. T.; Roth, W. J.; Leonowicz, M. E.; McCullen, S. B.; Hellring, S. D.; Beck, J. S.; Schlenker, J. L.; Olson, D. H.; Sheppard, E. W. *Chem. Mater.* **1994**, *6*, 2317.
(18) Zhao, D.; Goldfarb, D. *J. Chem. Soc., Chem. Commun.* **1995**, 875.
(19) Huo, Q.; Margolese, D. I.; Stucky, G. D. *Chem. Mater.* **1996**, *8*, 1147.
(20) Monnier, A.; Schüth, F.; Huo, Q.; Kumar, D.; Margolese, D.; Maxwell, R. S.; Stucky, G. D.; Krishnamurty, M.; Petroff, P.; Firouzi, A.; Janicke, M.; Chmelka, B. F. *Science* **1993**, *261*, 1299.

10.1021/cm980440d CCC: $15.00
Published on Web 10/29/1998

to the less reliable synthesis of MCM-48 compared to MCM-41. However, MCM-48 with three-dimensional channels seems more attractive than MCM-41 with one-dimensional channels for catalytic applications since MCM-48 can better avoid pore blockage during catalytic reactions.

Siliceous MCM-48 materials can be synthesized from gels with a wide range of surfactant/silicon (Surf/Si) ratios.[1,2,17−21] At a Surf/Si ratio of 0.12 MCM-48 and Mn-MCM-48 are synthesized in 3 days but various intermediate mesophases are observed dependent on the reaction temperature.[18] At a Surf/Si ratio of 0.24 MCM-48 is synthesized by mixed divalent and alkyltrimethylammonium surfactants after 8−9 days.[19] At a Surf/Si ratio of 0.65, MCM-48 is obtained after 3 days.[20] At a Surf/Si ratio of 0.8 MCM-48 is formed after 2−4 days.[21] Once the initial pH values vary slightly from those specified in each synthesis recipe, MCM-48 is not formed. The formation of MCM-48 also depends on mesophase transformations since the initially generated mesophase is not cubic.[18,19,21] No MCM-48 was thus far synthesized at room temperature. However, cubic MCM-48 can be successfully produced by posttreatment of hexagonal MCM-41.[22,23] In this work the dependence on initial synthesis conditions and the mesophase transformation sequence in the MCM-48 synthesis are studied and a repeatable synthetic method is developed. The mesophase transformation sequence is affected by pH, surfactant content, and silica source. By consideration of the balance of forces in the inorganic silicate and organic surfactant interface,[19,26−29] the probable driving forces controlling mesophase transformation are identified. The mesophases are characterized by powder X-ray diffraction (XRD), ^{29}Si magic-angle-spinning (MAS) NMR, transmission electron microscopy (TEM), and N_2 adsorption.

Experimental Section

Synthesis. The sources of silicon were tetraethyl orthosilicate (TEOS, 99%), fumed silica (99.8%), and sodium silicate solutions (~27 wt % SiO_2). The structure-directing agents were cetyltrimethylammonium chloride (CTAC, 25 wt % in H_2O) and cetyltrimethylammonium bromide (CTAB). CTAC was used as received, but CTAB was used as 10 wt % solutions by dissolving CTAB into deionized water and heating to 308 K for 1 h. All these chemicals were obtained from Aldrich.

A typical synthesis gel was prepared by adding 10 mL of TEOS to an aqueous solution containing 88 g of CTAB solution (10 wt %) and 10 mL of 2 M NaOH (EM Industries). After being stirred for about 0.5 h, the resulting homogeneous mixture was crystallized under static hydrothermal conditions at 373 K in a Teflon bottle for 72 h. The molar composition of the initial gel mixture was $1{:}0.23{:}0.55{:}112SiO_2/Na_2O/CTAB/H_2O$. The product was filtered out, thoroughly washed with deionized water and air-dried overnight. Such as-synthesized samples were calcined at 823 K first in flowing nitrogen for 1 h and then in flowing oxygen for 14 h to remove the CTAB.

Other synthesis conditions including variation of reaction time from 0.1 to 336 h and of temperature at 293, 323, 343, 363, and 383 K were studied. Also, CTAC and other silica sources (fumed silica and sodium silicate solution) were tested.

Characterization. Powder XRD patterns were collected using a Philips 1840 powder diffractometer with Cu Kα radiation (40 kV, 25 mA) at 0.025° step size and 1 s step time over a $1.5° < 2\theta < 15°$ range. The samples were prepared as thin layers on metal slides.

For TEM observation, powder specimens were ground and deposited on a grid with a holey carbon film and rapidly transferred to a JEOL 2000 FX electron microscope with an accelerating voltage of 100 kV.

N_2 adsorption isotherms were measured at 77 K using a Micromeritics Gemini 2375 analyzer. The volume of adsorbed N_2 was normalized to standard temperature and pressure. Prior to adsorption, the samples were dehydrated at 573 K for 5 h. The specific surface area, A_{BET}, was determined from the linear part of the BET equation ($P/P_0 = 0.05-0.31$). The pore size distribution was calculated from the desorption branches of the N_2 adsorption isotherm and the Barrett−Joyner−Halenda (BJH) formula.[30−32] The mesopore (17−100 Å) parameters, the cumulative surface area, A_{BJH}, and the cummulative pore volume, V_{BJH}, were obtained from the pore size distribution curves. The specific mesopore diameter, D_{BJH}, was calculated as $4V_{BJH}/A_{BJH}$.

Solid-state NMR spectra were recorded at 9.4 T using a Chemagnetics CMX-400 spectrometer. ^{29}Si MAS spectra were measured at 79.45 MHz with 60° pulses and 600 s recycle delays using zirconia rotors 7.5 mm in diameter spun at 3 kHz. The chemical shifts are given in ppm from external tetramethylsilane (TMS).

Results

XRD. The mesophases originating from the same initial gels were sampled at different reaction times between 0.1 and 72 h under typical synthetic conditions and give the XRD patterns shown in Figure 1. As-synthesized and calcined samples are shown by solid and dotted lines, respectively. Only 0.1 h after all reactants were mixed together at 293 K, an initial precipitate is formed and shows a tubular mesostructure (H_0) with a d_{100} spacing of 35.7 Å (Figure 1a). The notation H_0 used here to represent this mesophase is based on the nomenclature used by Tiddy for surfactant liquid crystal phases[33] and by Fyfe et al. for mesophases.[22] Capital H designates tubular mesophases, L designates lamellar phases, and V designates MCM-48 material, while subscripts are used to distinguish similar phases produced at different reaction times.

The H_0 mesophase is maintained after stirring at 293 K for 1 h (Figure 1b). Continued synthesis at 373 K for 5 h (Figure 1c) forms phase H_1 which has larger d_{100} spacings of 39.4 Å. Upon calcination, these tubular mesophases show only a broad XRD peak corresponding to 32.5 Å (not shown), indicating that these mesophases

(21) Romero, A. A.; Alba, M. D.; Zhuo, W.; Klinowski, J. *J. Phys. Chem. B* **1997**, *101*, 5294.
(22) Fyfe, C. A.; Fu, G. *J. Am. Chem. Soc.* **1995**, *117*, 9709.
(23) Gallis, K. W.; Landry, C. C. *Chem. Mater.* **1997**, *9*, 2035.
(24) Zhang, W. Z.; Pinnavaia, T. J. *Catal. Lett.* **1996**, *38*, 261.
(25) Schmidt, R.; Junggreen, H.; Stöcker, M. *Chem. Commun.* **1996**, 875.
(26) Stucky, G. D.; Monnier, A.; Schüth, F.; Huo, Q.; Margolese, D.; Kumar, D.; Krishnamurty, M.; Petroff, P.; Firouzi, A.; Janicke, M.; Chmelka, B. F. *Mol. Cryst. Liq. Cryst.* **1994**, *240*, 187.
(27) Firouzi, A.; Schaefer, D. J.; Tolbert, S. H.; Stucky, G. D.; Chmelka, B. F. *J. Am. Chem. Soc.* **1997**, *119*, 9466.
(28) Firouzi, A.; Kumar, D.; Bull, L. M.; Besier, T.; Sieger, P.; Huo, Q.; Walker, S. A.; Zasadzinski, J. A.; Glinka, C.; Nicol, J.; Margolese, D.; Stucky, G. D.; Chmelka, B. F. *Science* **1995**, *267*, 1138.
(29) Firouzi, A.; Atef, F.; Oertli, A. G.; Stucky, G. D.; Chmelka, B. F. *J. Am. Chem. Soc.* **1997**, *119*, 3596.
(30) Tanev, P. T.; Vlaev, L. T. *J. Colloid Interface Sci.* **1993**, *160*, 110.
(31) Naono, H.; Hakuman, M.; Nakal, K.; *J. Colloid Interface Sci.* **1994**, *165*, 532.
(32) Barrett, E. P.; Joyner, L. G.; Halenda, P. P. *J. Am. Chem. Soc.* **1951**, *73*, 373.
(33) Tiddy, G. J. T. *Phys. Rep.* **1980**, *57*, 1.

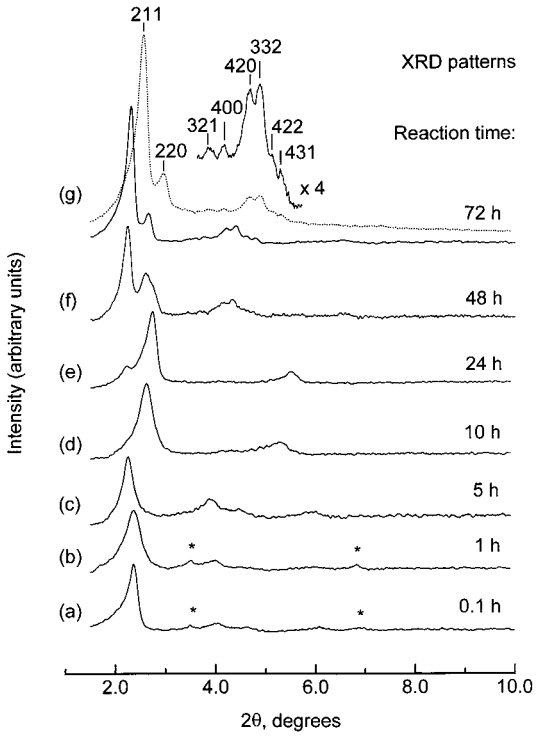

Figure 1. Powder XRD patterns of mesophases obtained at different reaction times during the formation of MCM-48: (a) 0.1 h; (b) 1 h; (c) 5 h; (d) 10 h; (e) 24 h; (f) 48 h; (g) 72 h. The solid lines are as-synthesized samples, and the dotted lines are calcined samples. The synthesis temperature is 293 K for (a) and (b) and 373 K for (c)−(g). The mesophases are (a)−(c) tubular, (d) pure lamellar, (e) and (f) lamellar and cubic mixtures, and (g) MCM-48.

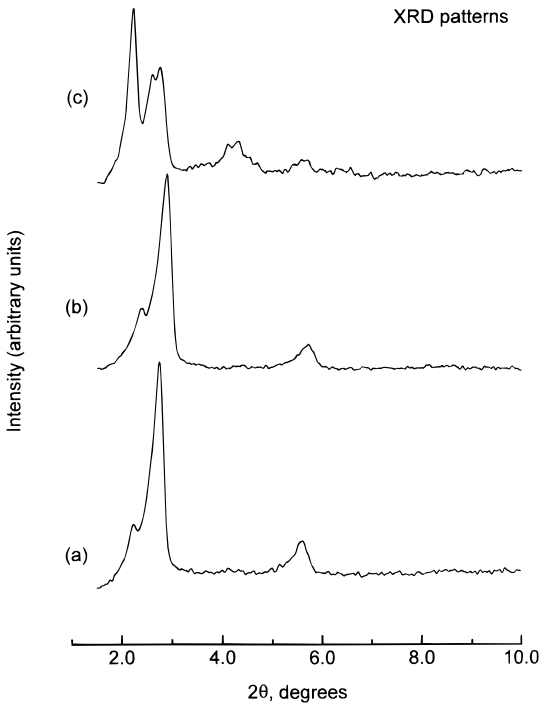

Figure 2. Powder XRD patterns observed for different parts of as-synthesized materials after hydrothermal synthesis at 373 K for 24 h: (a) entire product; (b) powder phase; (c) solid sphere phase.

are not very stable. The peaks marked by asterisks (∗) in Figure 1a,b are from crystalline CTAB.

After another 5 h hydrothermal reaction at 373 K, the H_1 mesophase converts into a lamellar phase with a d_{100} spacing of 33.8 Å (Figure 1d) which is designated L_1. This phase transformation from H_1 to L_1 is the first phase transformation. Further hydrothermal synthesis at 373 K for 24 h forms a cubic MCM-48 mesophase (V) (Figure 1e) which becomes the major product after 48 h (Figure 1f). After 72 h, this L_1 mesophase is transformed into pure MCM-48 mesophase (V) with a d_{211} spacing of 39.7 Å as shown by the solid line in Figure 1g. The XRD reflection peaks from 211 to 431 are all well resolved and in good agreement with reported patterns from pure siliceous MCM-48 materials.[1,17,19] The d spacings are compatible with the cubic $Ia3d$ space group[17,21] and the corresponding cubic unit cell parameter a is 97.2 Å based on the equation $a = d_{211}(6)^{-1/2}$. Upon calcination, shown by the dotted line in Figure 1g, the intensity of the XRD peaks increases by about 2.7 times compared to an as-synthesized sample, indicating that the degree of ordering is improved by the removal of the surfactant. The d_{211} spacing decreases to 34.2 Å and the corresponding cubic unit cell parameter contracts to 83.8 Å when surfactant cations are replaced by protons and the adjacent silanol groups condense. This transformation from L_1 to V is the second phase transformation.

At an early stage of the second transformation (∼ 24 h), the product is not simply a mixture of L_1 and V mesostructures (Figure 2a) but consists of two different morphologies. One is a very fine powder and the other is 3.5 mm diameter solid spheres. After careful separation of these by sieves, different XRD patterns are observed from these two morphologies (Figure 2). The fine powder shows an XRD pattern similar to the pure L_1 lamellar phase (Figure 2b), whereas the spheres show a dominate MCM-48 (V) structure (Figure 2c). The sphere morphology is about 20 wt % of the total product. During the hydrothermal synthesis, ethanol is produced from hydration of TEOS and remains in the reaction system since there is no total volume loss. However, once cosolvent ethanol is allowed to evaporate only a hexagonal mesophase is obtained.

The cubic mesostructure (V) is stable for 120 h (Figure 3a), but is later changed into a mixture of cubic and lamellar mesophases after 144 h (Figure 3b). After 168 h, the product is a pure lamellar mesophase (Figure 3c) which is designated as L_2 with a d_{100} spacing of 33.8 Å which is the same spacing as for the L_1 mesophase. This transformation from V to L_2 is the third phase transformation.

During these three mesophase transformations, the surfactant content and pH change as summarized in Table 1. The surfactant content in Table 1 is measured by comparing the weight loss between an as-synthesized sample pretreated at 373 K for 24 h and freshly calcined ones. It is found that the surfactant contents are around 50 wt % of the mesophases produced during the first two transformations, but decrease substantially to as low as 40 wt % in the L_2 mesophase after the third phase transformation.

The reaction system pH values also slightly change during these transformations as shown in Table 1. The initial pH value is 11.8 in an H_0 reaction mixture and remains similar in both H_1 and L_1 product solutions. But the pH increases to 12.0 in MCM-48 (V) product

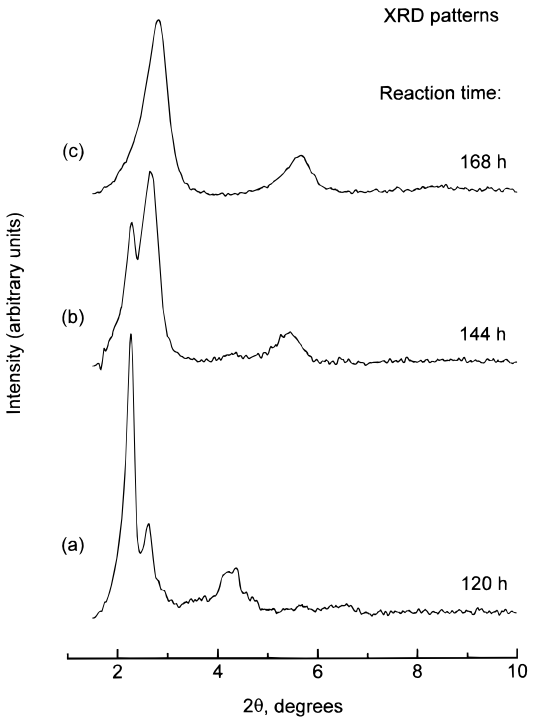

Figure 3. Powder XRD patterns of as-synthesized materials at 373 K for various times: (a) 120 h; (b) 144 h; (c) 168 h.

Table 1. Various Pure Mesophases and the Corresponding Synthesis System Parameters Such as Surfactant Content and pH Observed at Different Synthesis Times

reacn times (h)	mesophase structures	surfactant content in products (wt %)	pH of resulting solutions
0.1	tubular (H_0)	51	11.77
5	tubular (H_1)	50	11.78
10	lamellar (L_1)	48	11.76
72	cubic (V)	49	11.97
168	lamellar (L_2)	40	11.76

solutions after 72 h reaction. This suggests that the formation of MCM-48 is accompanied by consuming acids, which is consistent with a shift of the silica polymerization equilibrium due to pH adjustment by Ryoo et al.[34] It is interesting that once the V mesophase is totally transformed into the L_2 phase, the pH value becomes 11.8 again. So the formation of the L_2 phase consumes hydroxyl groups. Because the total reactant volumes are the same before and after hydrothermal reaction, the pH fluctuation is the result of the hydrothermal reaction.

To clarify the effect of hydroxyl ions on the third transformation, after formation of the V mesophase, the reactant mixture was cooled to 303 K, titrated by acetic acid solution to pH ~ 11.0, and then heated to 373 K for a total reaction time of 168 h. It was found that only pure V mesophase is produced which confirms that this acid treatment can inhibit the third transformation. So the existence of hydroxyl ions seems critical for the third mesophase transformation.

^{29}Si MAS NMR. The mesophases involved in the three transformations can be distinguished by ^{29}Si MAS NMR. Figure 4 shows the ^{29}Si NMR of the synthesis gel versus reaction time from 0.1 h (H_0) to 72 h (V). The

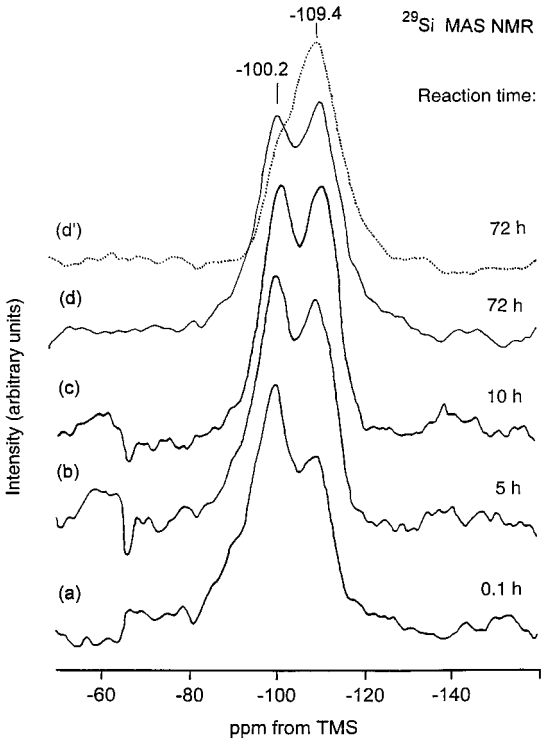

Figure 4. ^{29}Si MAS NMR spectra of as-synthesized (solid lines) and calcined (dotted lines) samples as in Figure 1 at different reaction times: (a) 0.1 h; (b) 5 h; (c) 10 h; (d), (d′) 72 h. The reaction temperature was 293 K for (a) and 373 K for (c)−(d).

spectrum of the initial tubular H_0 mesophase (Figure 4a) shows three broad peaks near −91 ppm from Q_2 silicons in $Si(OSi)_2(OH)$ units, near −101 ppm from Q_3 silicons in $Si(OSi)_3OH$ units, and near −110 ppm from Q_4 silicons in $Si(OSi)_4$ units.[21] Here Q stands for a silicon atom bonded to four oxygen atoms forming a SiO_4 tetrahedron and the subscript *n* indicates the number of other Q units attached to this unit.

The ^{29}Si MAS NMR spectra of as-synthesized H_1, L_1, and V mesophases are shown in Figure 4b−d. At the early stage of reaction when only tubular mesophases H_0 and H_1 exist, the most intense peak is the Q_3 line (Figure 4a,b). This indicates a low condensation state of the silanol groups which results in thermal unstability to calcination of these mesophases. The silicons in the L_1 phase are also less condensed as indicated in Figure 4c where the Q_3 peak is still as intense as the Q_4 peak. Once pure mesophase V is formed after 72 h, the Q_4 line becomes the most intense (Figure 4d) and only two peaks near −100.2 ppm and −109.4 ppm are observed, reflecting progressive silanol condensation during the formation of the MCM-48 mesophase. After calcination, the intensity of the Q_4 peak is substantially increased and the Q_3 peak almost disappears (Figure 4d′). In addition, these ^{29}Si MAS NMR spectral peaks in Figure 4 are broad, which indicates that the local atomic arrangement in the silica network of these mesophases is not uniform.

As indicated by XRD, after 24 h hydrothermal synthesis two solid morphologies are present. The corresponding ^{29}Si MAS NMR spectra (Figure 5) of these two morphologies show different degrees of silicon condensation based on the Q_3/Q_4 ratios of 0.83 for the fine powder (Figure 5a) and 0.64 for the solid spheres

(34) Ryoo, R.; Kim, J. M. *J. Chem. Soc., Chem. Commun.* **1995**, 711.

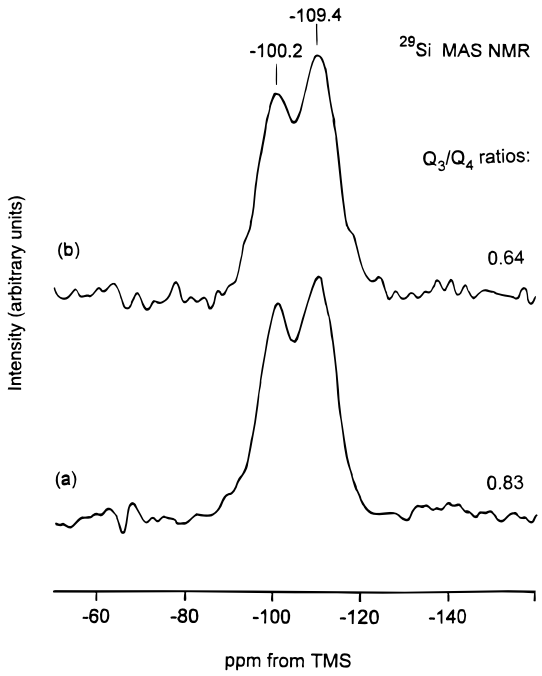

Figure 5. ^{29}Si MAS NMR spectra of different morphologies of as-synthesized samples as indicated in Figure 2: (a) powder phase; (b) solid sphere phase.

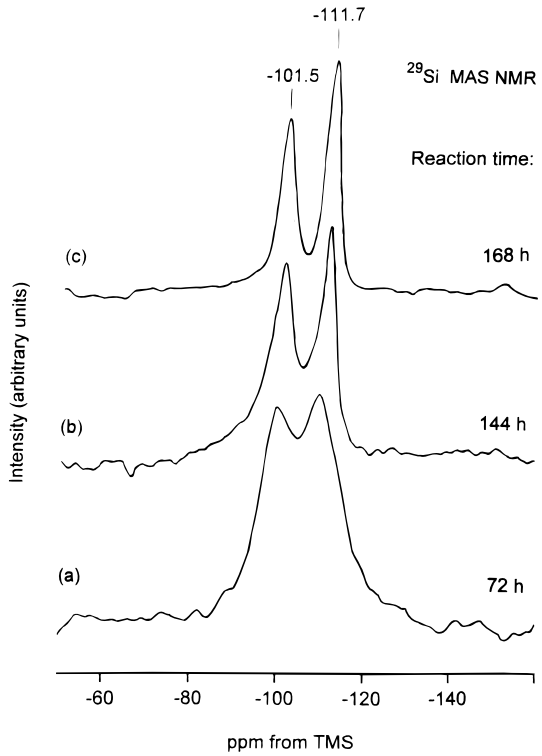

Figure 6. ^{29}Si MAS NMR spectra of samples corresponding to Figure 3 at different reaction times: (a) 72 h; (b) 144 h; (c) 168 h.

(Figure 5b). This indicates that the sphere morphology is more condensed than the fine powder.

After the third mesophase transformation, the ^{29}Si MAS NMR spectra are shown in Figure 6. The ^{29}Si MAS NMR peaks become sharp as soon as the V mesophase (Figure 6a) is transformed into the L_2 lamellar phase (Figure 6b,c). This indicates that the local atomic arrangement of the silica network in the L_2 lamellar phase is much more uniform than in the V mesophase.

Table 2. Q_3/Q_4 Ratios Calculated from ^{29}Si MAS NMR Spectra of Various Mesoporous Products Sampled at Different Reaction Times

reacn times (h)	mesophase structures	Q_3/Q_4 ratio
0.1	H_0	1.68
5	H_1	1.18
10	L_1	1.00
24	V + $(L_1)^a$	0.64
24	L_1 + $(V)^a$	0.83
72	V	0.94
144	V + L_2	0.94
168	L_2	0.83

[a] A trace of this mesophase also exists.

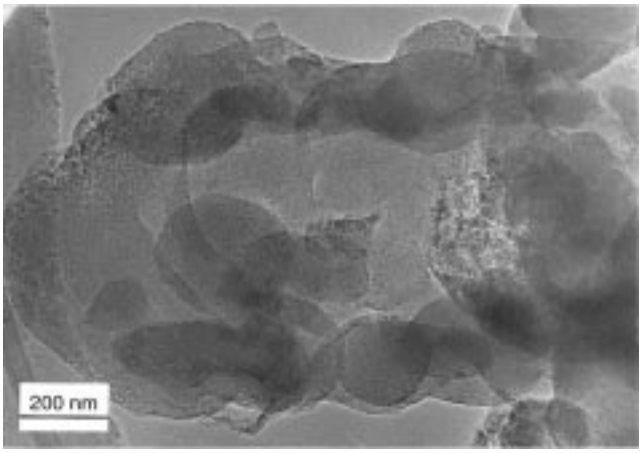

Figure 7. TEM image showing the appearance of MCM-48 particles.

To compare the relative amounts of silica condensation among the mesophases, Q_3/Q_4 ratios are shown in Table 2. The Q_3/Q_4 ratios for the H_0, H_1, and and L_1 mesophases are all above one and the MCM-48 mesophase has a Q_3/Q_4 ratio less than one indicating that the framework of the V mesophase is more condensed. The polymerization degree of framework silica in the two morphologies produced after 24 h is much higher than either the L_1 lamellar phase or the MCM-48 V phase indicating that the degree of silica polymerization fluctuates during the second phase transformation. However, the degree of silica condensation does not change so much during the third transformation. The Q_3/Q_4 ratios for the V mesophase and the V + L_2 mixture (144 h) are all 0.94 and decrease to 0.83 after V is totally transformed into the L_2 phase after 168 h. The silica in the L_2 lamellar phase is more condensed than the L_1 lamellar phase based on the Q_3/Q_4 ratios.

TEM. The structure of the MCM-48 mesophase was also characterized by high-resolution transmission electron micrographs shown in Figures 7−10. Calcined samples were used for TEM data since the stability of the samples in the microscope is noticeably enhanced after calcination.

Figure 7 is a low-resolution TEM image of several MCM-48 particles which show well-defined edges and a spherical shape. High-resolution TEM images for selected particles along the [100], [111], and [110] directions (Figures 8−10) match well with reported MCM-48 images.[21,35−37] Along the [100] direction the TEM micrograph (Figure 8) shows uniform pore struc-

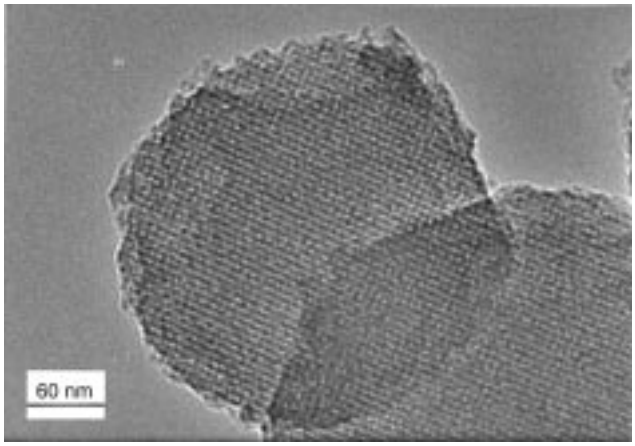

Figure 8. TEM image of calcined MCM-48 recorded along the [100] direction.

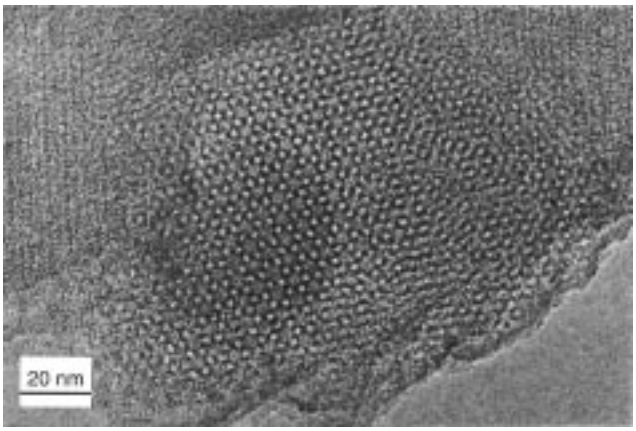

Figure 9. TEM image of calcined MCM-48 recorded along the [111] direction.

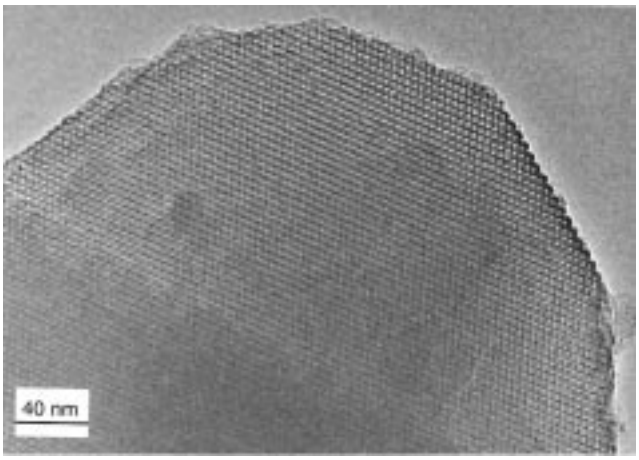

Figure 10. TEM image of calcined MCM-48 recorded along the [110] direction.

tures, while along the [111] direction (Figure 9) the image shows a well-defined hexagonal arrangement. Along the [110] direction (Figure 10) a very regular pattern without irregularities is observed. Along the [100] and [111] directions channels are observed, but along the [110] direction the contrast variation is due only to changes in electron density. Therefore, the [100] and [111] projections reflect the actual shape and structure of the channels, while the regularity of the TEM image in the [110] direction in Figure 10 indicates a uniform channel system. Although there is a slightly

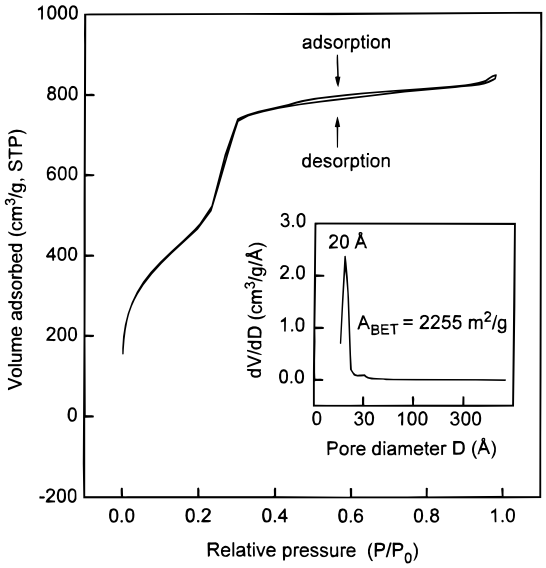

Figure 11. Adsorption−desorption isotherm of nitrogen at 77 K on calcined MCM-48. The insert shows the BJH pore size distribution calculated from the desorption branch of the isotherm.

uneven projection pattern along [100] in Figure 8 due to misalignment along the [100] direction,[21] a square pattern of dots still can be observed in some areas of this pattern and the cubic unit parameter *a* can be directly measured as about 83 Å from the hexagonal patterns[21,35] along the [111] direction in Figure 9. This is consistent with the XRD results.

N_2 Adsorption Isotherms. Low-temperature nitrogen adsorption isotherms enable the calculation of the specific surface area, pore volume, and mesopore size distribution. The N_2 adsorption isotherm for the calcined MCM-48 (V) materials is shown in Figure 11. It is a typical reversible type IV adsorption isotherm as defined by IUPAC.[38] A sharp inflection between relative pressure $P/P_0 = 0.2$ and 0.3 corresponds to capillary condensation within uniform mesopores. The sharpness of this step reflects the uniform pore size. Also, the fact that the initial region can be extrapolated back to the origin confirms the absence of any detectable micropore filling at low P/P_0. Therefore, a very uniform mesopore system without micropore structure is observed in the calcined samples. No defined hysteresis loop[39] in the adsorption and desorption cycle upon pore condensation is observed, which can be attributed to the small size of the particles as confirmed by TEM.[21,40]

The BJH plot of the derivative of the pore volume per unit weight with respect to the pore diameter (dV/dD) versus the pore diameter is shown in the inserted graph in Figure 11. A very narrow pore size distribution with an average pore diameter of 24 Å is observed. The BET surface area was calculated[39] with a 16.2 Å cross-

(35) Anderson, M. W. *Zeolites* **1997**, *19*, 220.
(36) Alfredsson, V.; Anderson, M. W. *Chem. Mater.* **1996**, *8*, 1141.
(37) Alfredsson, V.; Anderson, M. W.; Ohsuna, T.; Terasaki, O.; Jacob, M.; Bojrup, M. *Chem. Mater.* **1997**, *9*, 2066.
(38) Brunauer, S.; Deming, L. S.; Deming, W. S.; Teller, E. *J. Am. Chem. Soc.* **1940**, *62*, 1723.
(39) Sing, K. S. W.; Everett, D. H.; Haul, R. A. W.; Moscou, L.; Pierotti, R. A.; Rouquerol, J.; Siemieniewska, T. *Pure Appl. Chem.* **1985**, *57*, 603.
(40) Luan, Z.; He, H.; Zhou, W.; Cheng, C. F.; Klinowski, J. *J. Chem. Soc., Faraday Trans.* **1995**, *91*, 2955.

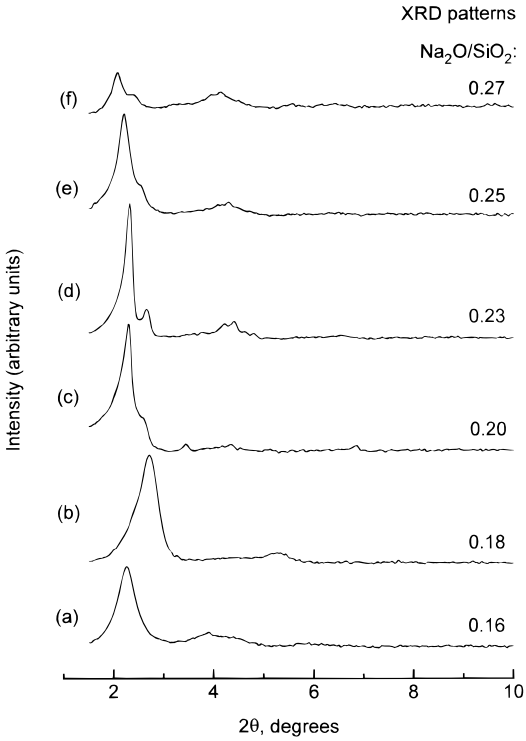

Figure 12. Powder XRD patterns of as-synthesized samples obtained at 373 K from initial gels with various amounts of NaOH. The Na_2O/SiO_2 ratios are (a) 0.16, (b) 0.18, (c) 0.20, (d) 0.23, (e) 0.25, and (f) 0.27. The gel compositions are 1:0.05−0.32:0.55:112SiO_2/Na_2O/CTAB/H_2O.

sectional area of nitrogen and is as high as 2255 m^2/g in the MCM-48 sample.

Different Initial Synthesis Conditions. Because our synthesis approach for MCM-48 is repeatable, we can reliably study the effects of the initial synthesis conditions on the formation of MCM-48. The effects of pH, temperature, and surfactant and silicon sources were studied.

The pH of the initial synthesis gels was adjusted by varying the amount of NaOH slightly, and XRD patterns are shown in Figure 12. After hydrothermal reaction at 373 K for 72 h, the resulting mesophases are MCM-41 for Na_2O/SiO_2 ratios in the initial gels from 0.05 to 0.16 (Figure 12a), lamellar at a Na_2O/SiO_2 ratio of 0.18 (Figure 12b), and MCM-48 as the Na_2O/SiO_2 ratio increases from 0.20 to 0.27 (Figure 12c−f). For gels with Na_2O/SiO_2 ratios more than 0.27, no precipitates are obtained at 373 K. However, at room temperature (293 K) after the same synthesis gels react for 72 h, for Na_2O/SiO_2 ratios in the initial gels of 0.16−0.25, only MCM-41 is formed while, for a Na_2O/SiO_2 ratio of 0.27, only an amorphous phase is obtained (not shown). Therefore, the formation of MCM-48 is not only related to the pH but also to the temperature.

To test the temperature effect on the formation of MCM-48, the synthesis was studied at different temperatures from 293 to 383 K. The results show that at 293, 323, and 343 K, only MCM-41 is obtained after 72 h (not shown), whereas at 363−383 K, MCM-48 materials are produced. This indicates that the formation of MCM-48 is sensitive to the temperature. MCM-48 was not formed at temperatures above 383 K.

MCM-48 can also be synthesized by using CTAC to replace CTAB. But the XRD patterns of the resulting products are not as well resolved. When other silicon sources, such as fumed silica and sodium silicate, are used to replace TEOS, only hexagonal MCM-41 is obtained. So the formation of MCM-48 depends on the silica source.

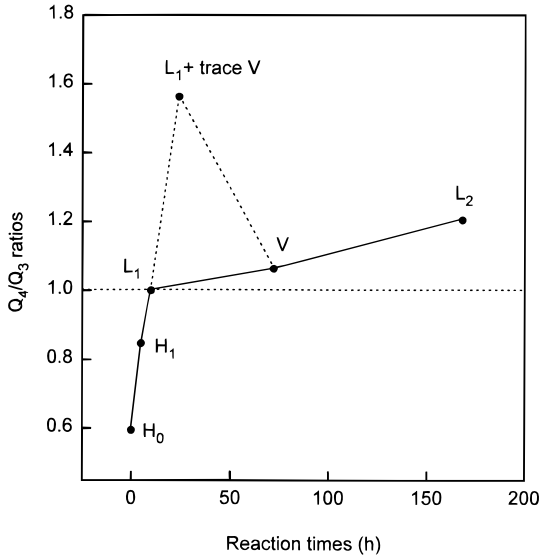

Figure 13. Q_4/Q_3 ratios in different mesophases calculated from ^{29}Si MAS NMR spectra.

Discussion

The mesophase transformations in the synthesis of MCM-48 occur versus reaction time in the sequence $H_1 \rightarrow L_1 \rightarrow V \rightarrow L_2$. The V phase (MCM-48) is an intermediate mesophase, which causes the synthesis of MCM-48 to be poorly repeatable and quite sensitive to the synthesis conditions.

Phase Transformation from H_1 to L_1. The first phase transformation is the fastest among the three transformations and is finished within only 5 h. The resulting L_1 mesophase still has a low degree of silica condensation although it is slightly increased compared to the H_1 phase (Figure 13). The surfactant contents in the solids and pH values in the reaction solutions remain the same during this transformation (see Table 1). Therefore, the driving force for this transformation seems not to involve these factors. However, the loss of ethanol cosolvent inhibits this transformation and indicates that the transformation is directly related to the presence of ethanol.

The transformation can be explained by a cooperative templating mechanism[6,19,26−29] in which the self-assembly of the organic−inorganic interface can be predicted by the surfactant packing parameter, $g = (V)/(a_0)(L)$,[19,26,41] where V is the total volume of the surfactant chain plus any cosolvent organic molecules between the chains, a_0 is the effective headgroup area at the organic−inorganic interface, and L is the kinetic surfactant chain length. Small values of g favor more curved surfaces such as MCM-41 ($^1/_3 < g < {}^1/_2$), while larger values favor structures with less curvature such as MCM-48 ($^1/_2 < g < {}^2/_3$) and layers ($g = 1$). Alcohol molecules with shorter alkyl chains (<4 carbons) tend to reside primarily in

(41) Israelachvili, J. N.; Mitchell, D. J.; Ninham, B. W. *J. Chem. Soc., Faraday Trans. 2* **1976**, *72* 1525.

the outer shell of a surfactant micelle.[6,19] This increases the effective surfactant volume *V* in the interface, raises the value of packing parameter *g*, and causes the formation of a lamellar phase when *g* increases to 1. Only MCM-41 is obtained when ethanol is allowed to evaporate during the synthesis which supports this argument. This is also consistent with the results that MCM-41 structures do not transform into other mesophases when no ethanol is added to the reaction system but do transform into a lamellar phase after adding the amount of ethanol produced from TEOS.[23]

Phase Transformation from L_1 to V. Unlike the H_1 to L_1 transformation, the L_1 to V transformation is kinetically slow and takes 62 h to complete. The ^{29}Si MAS NMR spectra indicate that the silanol groups are polymerized to a maximum degree when the V mesophase begins to form after 24 h (Figure 13, dotted lines), implying that sufficient silica condensation initiates the formation of MCM-48. So the polymerization of silica species is suggested to be the driving force for this transformation. The migration of ethanol occurs too rapidly to be very important in the L_1 to V transformation.

Silica condensation causes the negative charge density of the silicate network to decrease.[6,19] To maintain charge matching in the interface, the organic surfactants pack to form a high surface curvature to increase the effective headgroup area and lower the packing parameter so that the V mesostructure is favored. The variation of silica polymerization revealed by the dotted lines in Figure 13 reflects details of the second transformation. The first obvious increase of silicon condensation ($L_1 \rightarrow L_1$ + trace V, dotted line) shows the initial formation of the V mesostructure. The slight decrease (L_1 + trace V $\rightarrow$ V, dotted line) corresponds to reorganization of the L_1 phase. The silica polymerization consumes some acid and increases the pH which may prevent complete condensation of silica in MCM-48.

The second transformation is a heterogeneous process, and the solid sphere morphology transforms into the cubic V phase faster than the powder morphology. This is consistent with the degree of silica condensation being higher in the solid spheres than in the powder as indicated by ^{29}Si MAS NMR spectra in Figure 5.

Phase Transformation from V to L_2. The occurrence of the third transformation indicates that the framework silica of the V mesophase is not completely condensed as confirmed by Figure 13. Unlike the L_2 lamellar mesophase, the cubic mesophase is not a stable end product of the synthesis.

With formation of the L_2 phase, the pH decreases suggesting that some hydroxyl groups are consumed during the third transformation. Thus, this transformation can be inhibited by adjusting the pH. Therefore, the interaction of hydroxyl groups in the interface is suggested to be the driving force for this transformation.

The hydroxyl groups produced in the formation of MCM-48 interact with the silica or organic surfactant in the interface since the framework silica is already condensed. When hydroxyl groups interact with the surfactant in the interface, the hydrophobicity of the headgroup decreases so that the headgroup tends to remain in contact with water.[6,19] This decreases the effective cationic headgroup area and increases the surfactant packing parameter *g* which favors the formation of mesophases with low surface curvatures such as lamellar phases. In contrast, when extra hydroxyl groups interact with silica in the interface, the interfacial silica is less condensed and the negative charge density of the silica in the interface increases. So in order to maintain charge matching in the interface,[6,19] the surfactants rearrange to favor a low surface curvature as for the L_2 lamellar phase. During the V to L_2 mesophase transformation, the overall charge density of the silica in the L_2 phase decreases compared to the V phase. But it may increase in the interface due to a thicker silica wall in the L_2 mesophase as indicated by Fyfe et al.[22]

Suggested Formation Mechanism for MCM-48. The synthesis of MCM-48 is related to three mesophase transformations in the sequence $H_1 \rightarrow L_1 \rightarrow V \rightarrow L_2$ which are regulated by different driving forces, ethanol redistribution, silica condensation, and hydroxyl ion interaction, respectively. To reliably synthesize MCM-48 these driving forces must be controlled by adjusting the synthetic conditions.

The effect of different initial pH on the synthesis (Figure 12) can be explained since lower pH speeds up the kinetics of silica polymerization. At an initial Na_2O/SiO_2 ratio less than 0.16 (Figure 12a), silica polymerization is fastest and overcomes any effect of ethanol redistribution. So, only hexagonal MCM-41 material is produced (Figure 12a). For a Na_2O/SiO_2 ratio of 0.18 (Figure 12b), ethanol redistribution becomes relatively more important and the L_1 phase is formed. But this L_1 phase is probably too highly polymerized to further transform. So the L_1 phase is stabilized after 72 h (Figure 12b). For Na_2O/SiO_2 ratios greater than 0.27, the silica dissolves faster than it precipitates at 373 K, so no solid product is formed. Thus, only within a suitable range of initial Na_2O/SiO_2 ratios between 0.20 and 0.27 can the $H_1 \rightarrow L_1$ and $L_1 \rightarrow V$ transformations occur and MCM-48 be formed (Figure 12c−f).

This transformation sequence can also explain the temperature dependence. At room-temperature ethanol does not redistribute fast enough to dominate silica condensation and drive the H_1 mesophase to rearrange to the L_1 phase. At temperatures below 343 K, silica condensation is too slow to initiate the formation of MCM-48. At temperatures from 363 to 383 K silica condensation is accelerated and MCM-48 can be synthesized. So higher temperature is required for the synthesis of MCM-48. The effect of the silica source can also be explained. MCM-48 is not synthesized from other silica sources such as fumed silica and silica gel since no ethanol is formed which is required for the first transformation of H_1 to L_1.

The transformation sequence can also explain much previous work on the synthesis of MCM-48 materials. MCM-48 was synthesized at a low surfactant/silica ratio (0.12).[18] A relatively high ethanol content is expected for this low surfactant/silica ratio so the $H_1 \rightarrow L_1$ transformation occurs faster than in our synthetic system. Silica condensation needs to be slower to avoid the framework of the L_1 lamellar phase from becoming too condensed before the cubic phase V is initiated. This is achieved by higher pH ($Na_2O/SiO_2 = 0.30-0.34$) than used in our MCM-48 synthesis. At a surfactant/silica

ratio of 0.65 Monnier et al.[20] synthesized MCM-48 materials for a Na_2O/SiO_2 ratio of 0.25. This is similar to our synthesis. At a surfactant/silica ratio of 0.8 to 1.2, Romero et al.[21] observed similar transformations to ours. The initial mesophases were hexagonal MCM-41 and the cubic MCM-48 phase was also transformed to a lamellar phase.

Conclusions

A reliable synthesis of cubic MCM-48 materials is described which involves a mesophase transformation sequence involving hexagonal phase (H_1) transforming to a lamellar phase 1 (L_1) transforming to cubic MCM-48 (V) transforming to lamellar phase 2 (L_2). The driving forces for each transformation involve ethanol redistribution, silica condensation, and hydroxyl ions, respectively. The effect of temperature and pH on the synthesis can be rationalized by this sequence. In this transformation sequence phase V is MCM-48, which is an intermediate mesophase. This is why synthesis of cubic MCM-48 is very sensitive to the reaction conditions.

Acknowledgment. This research was supported by the Robert A. Welch Foundation, the University of Houston Energy Laboratory, and the National Science Foundation.

CM980440D